Pergamon

Int. J. Multiphase Flow Vol. 24, No. 1, pp. 55–75, 1998

Printed in Great Britain
PII: S0301-9322(97)00043-8
0301-9322/98 $19.00 + 0.00

A TURBULENT DIFFUSION MODEL FOR PARTICLE DISPERSION AND DEPOSITION IN HORIZONTAL TUBE FLOW

B. MOLS and R. V. A. OLIEMANS

J.M. Burgers Centre for Fluid Mechanics, Laboratory for Aero- & Hydrodynamics, Delft University of Technology, Delft, The Netherlands

(Received 11 September 1996; in revised form 27 May 1997)

Abstract—Particle dispersion and deposition in a horizontal turbulent tube flow have been studied with a Turbulent Diffusion Model. Dispersion and deposition are modelled as the combined process of turbulent diffusion and gravitational settling fluxes. The particle diffusion coefficient is expressed in terms of the fluid diffusivity, taking into account the inertial effect and the crossing trajectories effect. The analytical solution for the particle concentration in a one-dimensional problem between two horizontal plates is found, and is used to calculate the relative deposition between the top and the bottom wall. It is investigated how this relative deposition depends on the particle diameter, the height of the channel and the Froude number. The one-dimensional analytical solution is used to predict the two-dimensional deposition flux in a tube, and it is investigated how this depends on the particle diameter and the Froude number. The expression for the deposition flux contains the characteristic physical parameters of the deposition problem that have not been recognized in earlier work. © 1997 Elsevier Science Ltd

Key Words: particle deposition, particle dispersion, deposition rate, turbulent diffusion, annular flow, horizontal flow

1. INTRODUCTION

The importance of dispersion and deposition of particles has been recognized in industrial and environmental applications as well as in science. Transport of pollution in the atmosphere or in the oceans, transport of sediment in rivers and oceans, inhalation of toxic dusts, deposition during microchip fabrication, air or water cleaning, catalyst particles in riser flows and droplet deposition in annular dispersed two-phase flows are some examples. Annular dispersed flow is the prevailing flow regime during the production of gas and in thermal cracking processes in furnace tubes. In all these examples one is interested in how particles or droplets are transported and what determines their deposition on some boundary.

In this paper we are concerned with one of these examples, namely a horizontal annular dispersed gas/liquid flow in a tube. In these flows, the core of turbulently flowing gas contains liquid in the form of droplets with diameters between 10 and 1000 μm (1 mm). The droplets are entrained from the liquid film, and can deposit at various positions on the annular film. Figure 1 gives a sketch of this entrainment/deposition mechanism in a horizontal annular dispersed gas/liquid flow in a tube. It is one of the mechanisms that have been proposed to explain the annular character of the film. Other mechanisms that have been proposed are wave spreading, secondary gas flow, and surface tension (Fukano and Ousaka 1989; Laurinat *et al.* 1985).

Till now it is not clear which mechanism, or which combination of mechanisms is/are responsible for the annular character of the film. Instead of immediately solving the basic liquid film equations for conservation of mass and momentum, where empirical correlations or simple models are needed for all the four mentioned mechanisms (Fukano and Ousaka 1989; Laurinat *et al.* 1985), we study only the deposition mechanism, separately from the other mechanisms. This should lead to an expression for the deposition flux with a wider range of applicability than the correlations that have been used so far. In the following we speak about particles and not about droplets, as in our analysis the behaviour of droplets does not differ from the behaviour of solid, hard spherical particles.

In order to solve the basic liquid film equations for a horizontal annular dispersed gas/liquid flow, the flux of depositing particles at a certain circumferential angle in the tube has to be known (Fukano and Ousaka 1989; Laurinat *et al.* 1985). Except for very large particles ($>200\ \mu$m), for which the motion is totally dominated by gravity and the particle's initial entrainment velocity (Anderson and Russell 1970; James *et al.* 1987), there is at present no theoretical analysis of this deposition flux in a two-dimensional geometry. Anderson and Russell (1970) developed a semi-empirical expression to correlate deposition and entrainment fluxes, but only for the top half in the tube. The model used to derive this expression assumes that droplet deposition is caused by deterministic drop trajectories intersecting the liquid film. The work of James *et al.* (1987) is an extension of the work of Anderson and Russell (1970). In both approaches no effect of turbulence was taken into account because only very large particles were considered. Laurinat *et al.* (1985) proposed an empirical fit to a representative deposition flux profile measured by Anderson and Russell:

$$R_D(\phi) = k_D[1 + 10\exp(2(\cos\phi - 1))], \qquad [1]$$

where R_D is the deposition flux, k_D is a constant that has to be calculated from the entrainment of particles, and ϕ is the angle around the tube circumference. Figure 2 gives a sketch of this correlation in units of k_D. Deposition is the highest at the bottom and the lowest at the top. In all horizontal annular flow models up till now a correlation like [1] or even a more simple deposition flux, not depending on the circumferential tube angle, has been used.

However, it is clear that the behaviour of $R_D(\phi)$ must depend on the gas velocity. The difference between deposition at the bottom and deposition at the top is expected to decrease with increasing gas velocity. Unfortunately, correlation [1] does not depend on the characteristic physical parameters of the problem. Its applicability is restricted to conditions not far removed from those for which the constants have been determined. In this study we investigate whether or not a more generalized form of this equation can be derived using a turbulent diffusion model (Binder and Hanratty 1992).

The history of the Turbulent Diffusion Model presented in this paper goes back to Taylor (1921) and to Friedlander and Johnstone (1957). Taylor (1921) introduced the concept of Turbulent Diffusion in a study of the spread of scalar properties like smoke, heat and soluble matter. Friedlander and Johnstone (1957) used this concept for modelling a two-phase flow with particles. They also introduced the "diffusion/free-flight" concept (explained later) for particles depositing at a wall. In order to improve agreement with experimental data, different modifications of this

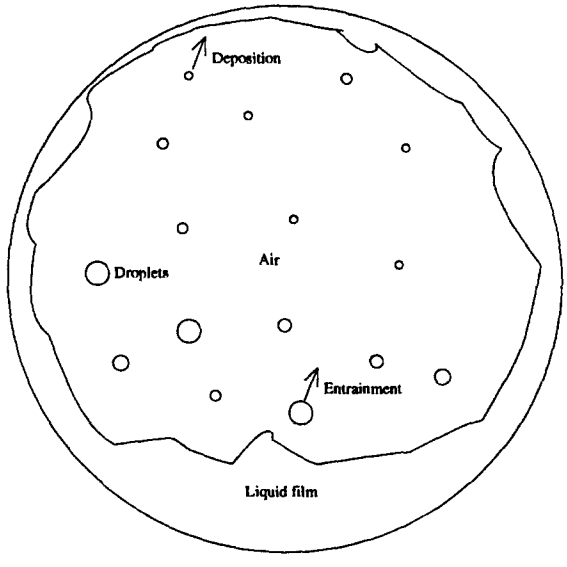

Figure 1. The entrainment/deposition mechanism in a horizontal tube.

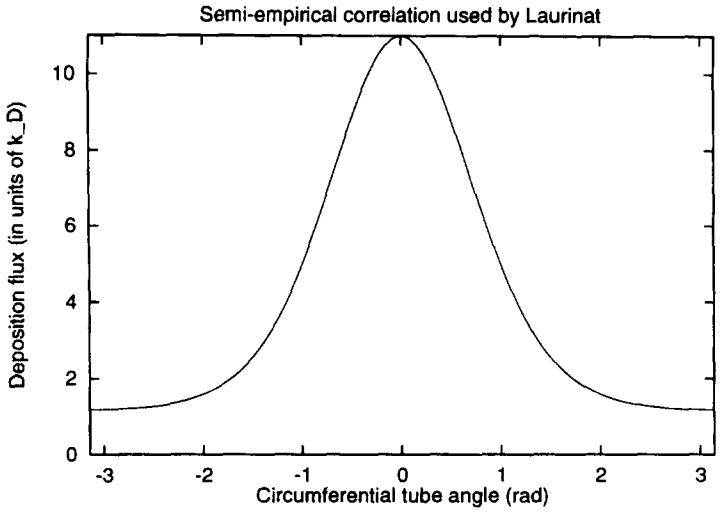

Figure 2. The deposition flux in a tube as a function of the circumferential angle in the tube. ($\phi = 0$ is the bottom, $\phi = \pm\pi$ is the top).

concept were proposed in the course of time: varying free-flight distance from the wall; modifying free-flight velocity; particle diffusivity unequal to eddy diffusivity; changing concentration boundary condition at the free-flight distance (Kallio and Reeks 1989).

The most recent contribution in the field of particle deposition described in the framework of turbulent diffusion is the work of Binder and Hanratty (1992), which is the starting point of this article. They considered the dispersion and deposition of particles in a two-dimensional horizontal rectangular channel by a convection/diffusion model. The diffusion part of this model represents the influence of turbulence and the convection part represents the influence of gravity on the particles. Particles are emitted from an instantaneous point source at the bottom of the channel with some initial entrainment velocity and can deposit at either of the perfectly absorbing boundaries. The particle diffusivity and the particle deterministic fall velocity are taken to be functions of the time that a particle has been in the flow field. The resulting convection/diffusion equation and the equation for the time-dependent deterministic velocity of the particles are solved numerically. One of their conclusions is that two dimensionless groups determine the resulting concentration profiles: the ratio of the time scale of the particle to the time scale of the fluid, τ_p/T_L, and the Froude number based on the friction velocity, Fr*. τ_p is the particle relaxation time and T_L is the integral fluid time scale. The Froude number is defined by Binder and Hanratty (1992) as $(u^*)^2/gH$, with u^* the friction velocity, g the acceleration of gravity, and H the height of the channel. For small Fr* T_L/τ_p the deposition flux is controlled by gravitational settling, whereas for large Fr* T_L/τ_p it is controlled by the turbulence of the fluid.

The main differences between the method used in this paper and the approach of Binder and Hanratty (1992) are two-fold. First, we assume the particle diffusion coefficient and the gravitational settling velocity to be stationary instead of time-dependent. This assumption has the great advantage that the one-dimensional problem can then be solved analytically, so that we find a general expression for the deposition flux independent of the exact quantitative modelling of the particle diffusion coefficient and the gravitational settling velocity. It furthermore has the advantage that an analytical two-dimensional deposition flux in a tube can be calculated which contains the relevant physical parameters of the problem that are hidden in generally used empirical correlations like [1]. Of course it has the disadvantage of not taking into account the fact that the particle deterministic velocity is generally time-dependent and that the particle diffusion coefficient is initially also time-dependent. Second, we explicitly include the inertial and crossing trajectories effects in the particle diffusion coefficient. Thus the particle diffusion coefficient is equal to the fluid diffusivity for $\tau_p/T_L < 1$, but smaller than the fluid diffusivity for $\tau_p/T_L > 1$. Binder and Hanratty (1992) assumed the particle diffusion coefficient to be equal to the fluid diffusivity. They did not consider at all the crossing trajectories effect.

The rest of this paper is organized as follows. First, we will give a definition of the problem under consideration, specify the assumptions on which our model is based, and introduce the relevant length and time scales in the problem. Thereafter, we will specify a time-dependent, one-dimensional convection/diffusion problem, solve the accompanying equations analytically and finally use the solution to calculate one- and two-dimensional deposition fluxes of particles. The two-dimensional deposition flux will be compared with the semi-empirical correlation of Laurinat [1]. At the end of this paper we will draw the most important conclusions of our analysis and discuss these.

2. DEFINITION OF THE TURBULENT DIFFUSION PROBLEM

Between two infinite horizontal plates particles are dispersed by turbulence and convected by gravity and they can deposit at the walls. The problem is sketched in figure 3.

The streamwise turbulence is assumed to have little effect on the particle deposition at the walls, because the fluid mean velocity is dominant in the streamwise direction. It is assumed that particles can cross the boundary layers at the walls on their inertia. The radial fluctuating velocity becomes almost constant for $y \cdot u^*/\nu_f > 50$, so that we define the beginning of the boundary layer at $y \cdot u^*/\nu_f = 50$. We study the time-dependent problem, with perfectly absorbing walls, and we consider two initial conditions: the initial condition at which all the particles are homogeneously distributed on a tube cross-section without having an initial radial velocity, and the initial condition of an instantaneous source at the bottom wall. Our aim is to predict from the Turbulent Diffusion Model the deposition flux of particles.

In the Turbulent Diffusion Model we make the following assumptions.

(1) Turbulent gas flow in a horizontal tube containing particles with a particle/fluid density ratio of the order of 1000 (simulating an air–water flow).

(2) No liquid film at the wall.

(3) Dilute particle suspension (volume fraction $O(10^{-6})$: one way coupling) without break-up and coalescence.

(4) Uniform and axial average fluid velocity (plug flow).

(5) Homogeneous turbulence up to the boundary layers.

(6) Perfectly absorbing walls.

(7) The particle mean free path (defined later) is larger than the thickness of the boundary layer (so that there is a free flight of particles through the boundary layer to the wall) and the particle mean free path is smaller than the tube diameter.

(8) We assume that Fick's law is valid, so that particles are in local equilibrium with the surrounding fluid, and a diffusion equation can be applied. For homogeneous turbulence this condition implies that the particle relaxation time must be much greater than the integral time scale of turbulence and much less than the particle diffusion time (Reeks 1983). The motion of the particles is then statistically similar to Brownian motion. These high inertia particles react slowly and with small amplitudes only on the large scale turbulent structures. Therefore they see the turbulent field more or less as a random field with little structure.

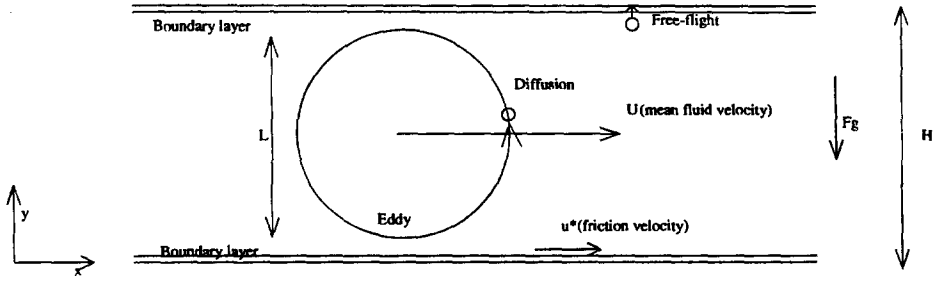

Figure 3. The diffusion/free-flight problem between two infinite horizontal plates.

Table 1. Length scales

Tube diameter	5×10^{-2} m
Eulerian eddy length scale	5×10^{-3} m
Kolmogorov length scale	O(100) μm
Particle diameter	10 μm $< d_p <$ 200 μm

(9) Stationary particle free fall velocity v_g.

(10) Particle diameters lie between 10 and 200 μm, so Brownian motion can be ignored and particle motion is not fully dominated by gravity.

These assumptions will be discussed at the end of this paper. We note that the assumptions of homogeneous turbulence and uniform, axial fluid velocity are more or less justified by assumption (10). High inertia particles effectively see almost homogeneous turbulence (they do not respond much to gradients in the fluid r.m.s. velocity normal to the walls), and they will not respond much to variations in the mean flow of the fluid.

Very important is a consideration of the relevant length and time scales in the problem. Table 1 gives the orders of magnitude of the relevant length scales: the diameter of the tube; the typical Eulerian eddy length scale; the smallest scale of the turbulent structures (the Kolmogorov length scale) and the diameter of the particle. The Kolmogorov length scale λ_K is calculated according to

$$\lambda_K \sim \left(\frac{\nu_f^3}{\epsilon}\right)^{1/4}, \qquad [2]$$

where ν_f is the kinematic viscosity of the fluid, and ϵ the kinetic energy dissipation, given by

$$\epsilon = k \cdot \frac{U^3}{L}. \qquad [3]$$

Velocity scale U is related to the friction velocity u^* and is approximately equal to one tenth of the average fluid velocity. Length scale L is approximately one tenth of the diameter of the tube, and for a tube $k \approx 0.01$.

The relevant time scales are the integral time scale T_L of the fluid and the particle relaxation time based on Stokes drag, τ_p. The integral time scale T_L of the fluid is given by

$$T_L = \int_{t_0}^{\infty} \frac{\langle v_f'(t) v_f'(t_0) \rangle}{\langle v_f'^2 \rangle} \, dt, \qquad [4]$$

where v_f' is the fluctuating velocity of the fluid and t_0 some initial time. In a tube flow, T_L will depend on the spatial position, but as homogeneous turbulence is assumed, T_L is taken to be constant. Approximately T_L can be calculated by

$$T_L \approx \frac{L}{U}. \qquad [5]$$

Of course there is in fact a whole range of time scales in turbulence. However, for the dispersion of particles the time scale T_L of the most energetic, large eddies is assumed to be dominant. The particle relaxation time based on Stokes drag is equal to

$$\tau_p = \frac{1}{18} \frac{d_p^2}{\nu_f} \frac{\rho_p}{\rho_f}, \qquad [6]$$

with ν_f the kinematic viscosity of the fluid, and ρ_p and ρ_f the densities of, respectively, the particle and the fluid. For particle Reynolds numbers larger than one, the real relaxation time will be smaller due to the increased drag in the non-Stokes case. The ratio τ_p/T_L is called the Stokes number S and can be interpreted as a measure of the influence of particle inertia on the dispersion of particles by fluid turbulence. Table 2 gives an overview of the orders of magnitude of the time scales τ_p and T_L.

We can distinguish three cases: the particle relaxation time is much smaller, of the same order of magnitude, or much larger than the fluid integral time scale, leading to different responses on the turbulent fluctuations, different behaviour in the boundary layer, and different deposition fluxes. For particle relaxation times much smaller than the fluid integral time scale ($S \ll 1$), particles precisely follow the velocity fluctuations of the fluid, the deposition is delayed by the boundary layer and the deposition flux is low all around the tube wall. As shown in table 2, in our case this holds for the 10 μm particles. For particle relaxation times of the same order of magnitude as the fluid integral time scale ($S \approx 1$), particles follow the turbulent fluctuations quite well, the effect of the boundary layer on the deposition is limited, and the deposition flux due to turbulence is high all around the tube wall. For particle relaxation times much larger than the fluid integral time scale ($S \gg 1$), the response to the turbulent fluctuations is slow, and the particles effectively see a randomly fluctuating velocity field. The deposition is not affected by the boundary layer, and the deposition flux is large at the bottom and small at the top, due to gravity. This is expected to hold for the 200 μm particles.

Annular dispersed gas/liquid flows in industrial processes often operate under different conditions from laboratory air–water flows. Pressures are often much higher as well as the physical dimensions of the tube. In order to know to what extent there is a dynamic similarity between a laboratory experiment and a field experiment, it is necessary to consider the characteristic dimensionless parameters. Whereas for an isothermal one-phase flow there is only one characteristic parameter, the Reynolds number, for two-phase flows there are five similarity parameters which determine a general isothermal two-phase flow problem (Chesters 1975): the Reynolds number, the Froude number, the Weber number, the density ratio and the viscosity ratio. There is a dynamic similarity between two gas/liquid flows if these five similarity parameters are the same, and if there is a geometrical similarity of the imposed boundary conditions. Table 3 gives the orders of magnitude of these five similarity parameters for the problem that we consider. We will assume that we have water droplets in a turbulent air flow. For calculating Reynolds and Froude numbers we have used a 45 m/s gas velocity and a tube diameter of 5×10^{-2} m. In the Weber number we have used the same gas velocity, but as length scale the typical diameter of a droplet, 100 μm, in order to have an estimate for the ratio of turbulent stress and surface tension. The surface tension between water and air is 73×10^{-3} N/m. Break-up of a fluid particle can only be expected for Weber numbers much larger than one.

3. MATHEMATICAL FORMULATION OF THE PROBLEM

The concept of a diffusion equation makes sense physically when the relevant length scale over which the diffusion process is considered (here the height of the channel) is larger than the particle mean free path (defined in homogeneous turbulence), and the time of observation is larger than the mean free time (T_L). Following Swailes and Reeks (1994) we can define a particle mean free path in a turbulent flow as the distance a particle travels in a time over which its motion is correlated. The particle mean free path l is then defined as

$$l = \sqrt{\langle v_p'^2 \rangle} T_p, \qquad [7]$$

with $\langle v_p'^2 \rangle$ is the particle mean square velocity and $T_p = T_L(1 + S)$ the particle integral time scale. With increasing particle relaxation time, the particle r.m.s. velocity decreases, but the correlation time of the particle velocity increases more than the particle r.m.s. velocity decreases. Figure 4 gives the ratio between tube diameter and mean free path, H/l, as a function of the particle diameter and for two different Froude numbers.

Table 2. Time scales

Integral fluid time scale	$O(10^{-3})$ s
Particle relaxation time ($d_p = 10$ μm)	$O(10^{-4})$ s
Particle relaxation time ($d_p = 200$ μm)	$O(10^{-1})$ s

Table 3. Orders of magnitude of the two-phase flow similarity parameters for our problem

Reynolds number	$O(10^5)$
Froude number	$O(10^3)$
Weber number	$O(1)$
Density ratio	$O(10^3)$
Viscosity ratio	$O(10^2)$

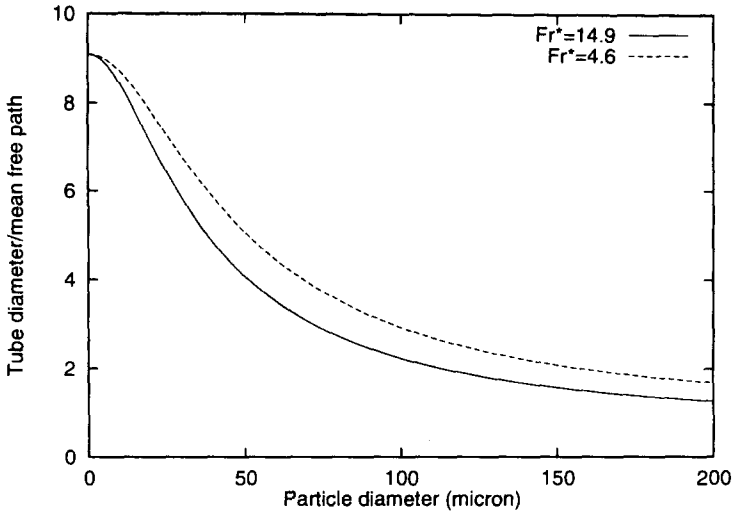

Figure 4. Ratio between tube diameter and particle mean free path as a function of particle diameter for $Fr^* = 4.6$ and $Fr^* = 14.9$ (5×10^{-2} m tube diameter).

Even for the largest particles that we use in our calculations, the 200 μm particles, this ratio is still larger than one, which supports assumption (7) in our Turbulent Diffusion Problem. In the limit of very small particles, the mean free path is assumed to be determined by the Eulerian integral length scale, which is 0.11 of the tube diameter. H/l is then approximately 9. In the limit of very large particles, the mean free path goes to infinity, and H/l goes to 0. The particle mean free path increases with increasing Froude number.

In inhomogeneous turbulence the gradient diffusion model, strictly speaking, is not valid unless $\tau_p^+ = \tau_p(u^*)^2/\nu_f \ll 3$ (Reeks 1983). For larger particle relaxation times than this limit, turbophoresis becomes important. Turbophoresis is the effect that in inhomogeneous turbulence particles migrate from a region of high turbulent velocity fluctuations to a region of low velocity fluctuations (Reeks 1983). We will, however, neglect it in our model, because we have assumed homogeneous turbulence.

As we have defined the physical problem and considered the relevant length and time scales, we can now derive a mathematical formulation of the problem. A time-dependent convection/diffusion equation in one spatial dimension is generally written as

$$\frac{\partial C(y,t)}{\partial t} = D_p \frac{\partial^2 C(y,t)}{\partial y^2} + v_G \frac{\partial C(y,t)}{\partial y}, \qquad [8]$$

where $C(y, t)$ is the particle concentration as a function of the spatial position y and time t. D_p is the particle diffusion coefficient and $v_g = g\tau_p$ the gravitational settling velocity of the particle. The first term on the right-hand side is the diffusive term due to the influence of turbulence on the particles, the second term is the convective term due to the influence of gravity on the particles. Following Binder and Hanratty (1992) we make variables dimensionless according to

$$y^+ \rightarrow \frac{y}{H}; \quad t^+ \rightarrow \frac{tu^*}{H}; \quad D_p^+ \rightarrow \frac{D_p}{u^*H}; \quad v^+ \rightarrow \frac{v}{u^*}; \quad C^+ \rightarrow \frac{Cu^*}{R_E}, \qquad [9]$$

where R_E is the entrainment flux of particles and u^* is the friction velocity. The friction velocity is calculated by using the Blasius correlation for a smooth tube

$$C_f = 0.0791 \cdot \mathrm{Re}_f^{-0.25}, \qquad [10]$$

where C_f is the friction coefficient, and Re_f the fluid Reynolds number. From the friction coefficient the wall shear stress τ_s is calculated as

$$\tau_s = \frac{1}{2}\rho_f V_G^2 C_f, \qquad [11]$$

where V_G is the average gas velocity in the tube. The wall shear stress is related to the friction velocity u^* by

$$u^* = \sqrt{\frac{\tau_s}{\rho_f}}. \quad [12]$$

The one-dimensional convection/diffusion equation for the concentration of particles C^+ can then be written in the dimensionless form

$$\frac{1}{D_p^+}\frac{\partial C^+}{\partial t^+} = \frac{\partial^2 C^+}{\partial (y^+)^2} + P\frac{\partial C^+}{\partial y^+}, \quad [13]$$

where the Peclet number P is defined by

$$\mathrm{P}: = \frac{g\tau_p}{D_p}\cdot H. \quad [14]$$

The Peclet number is the ratio of the convection term due to gravitational settling and the diffusion term due to turbulent diffusion. For Peclet numbers much smaller than one, turbulent diffusion is dominant, whereas for Peclet numbers much larger than one, gravitational settling becomes dominant. H is the height between the plates. We model the particle diffusion coefficient D_p by relating it to the fluid diffusivity D_f by

$$D_p = \gamma_{inert}\gamma_{cross}D_f, \quad [15]$$

where the fluid diffusivity is given by

$$D_f = \int_0^\infty \langle v_f'(0)v_f'(t)\rangle \, dt \approx \langle v_f'^2\rangle \int_0^\infty e^{-\frac{t}{T_L}} dt = \langle v_f'^2\rangle T_L \quad [16]$$

(Taylor 1921). The fluid mean square velocity $\langle v_f'^2\rangle$ can be approximated by $(0.7\cdot u^*)^2$ in the part of the tube where turbulence is considered to be homogeneous. From figure 15 in Uijttewaal and Oliemans (1996) it can be concluded that, in the absence of gravity, the ratio of particle and fluid diffusivity is governed by the ratio of particle relaxation time and fluid integral time scale. From this figure the inertial coefficient γ_{inert} can then be estimated as

$$\gamma_{inert} = \frac{1}{\sqrt{1+\frac{\tau_p}{T_L}}}. \quad [17]$$

Physically it corresponds to a decreasing response of particles on the fluid turbulence (in a wall bounded flow) if $\tau_p > T_L$. In the presence of a gravity field a crossing trajectories effect generally has to be taken into account according to Csanady (1963). A particle falling through an eddy loses its velocity correlation more rapidly than a fluid element. Thus it sees a fluctuating velocity field that varies more rapidly in time than a fluid element. The velocity correlation of a fluid element is determined only by the decay of an eddy. The result is that the crossing trajectories effect leads to a decreased particle diffusivity. It is determined by the ratio between the fluid integral time scale T_L and the time spent by a particle within an eddy, L/v_g with L the Eulerian eddy length scale and $v_g = g\tau_p$ the gravitational settling velocity. The crossing trajectories coefficient γ_{cross} is then given by

$$\gamma_{cross} = \frac{1}{\sqrt{1+\left(\frac{g\tau_p T_L}{L}\right)^2}}. \quad [18]$$

From this formula it can be calculated that for 200 μm particles the crossing trajectories effect can reduce particle diffusivity by about 10% for an average gas velocity of 32 m/s ($Fr^* = 4.6$), and by less than 5% for 62 m/s ($Fr^* = 14.9$). These gas velocities were chosen because for both gas velocities measurements have been done by Paras and Karabelas (1991) in a 5 cm tube. Figure 5

gives both the inertial coefficient and the crossing trajectories coefficient as a function of particle diameter for Fr* = 4.6 and Fr* = 14.9. The inertial effect is very important for the particles sizes under consideration, but the crossing trajectories effect is only significant for particles larger than about 150 μm. Diffusion coefficient [15] differs from the diffusion coefficient that was used by Binder and Hanratty (1992). The latter assume the particle diffusivity to be equal to the diffusivity of the fluid. This assumption is based on an experiment by Vames and Hanratty (1988). However, Vames and Hanratty only measured the ratio of particle and fluid diffusivity for Stokes numbers (τ_p/T_L) not larger than 2, whereas particles larger than 50 μm in an annular flow system have Stokes numbers significantly larger than 2 (see table 4 later). As Uijttewaal and Oliemans (1996) calculated the ratio of dispersion coefficients for Stokes numbers between 0.1 and 500, we use the results of their calculation to model the particle dispersion coefficient. This implies that the particle diffusion coefficient [15] decreases with increasing Stokes number for $S > 1$.

Because the particle mean free path is larger than the thickness of the boundary layer, a convection/diffusion equation is no longer valid for the particle behaviour in the boundary layer. It is assumed that particles are projected towards the wall at the beginning of the boundary layer, leading to a free-flight flux $v \cdot C$, where v has the dimensions of a velocity. The free-flight flux is then approximated by

$$v \cdot C = \int_0^\infty C \cdot v p(v)\, dv, \qquad [19]$$

where $p(v)$ is the velocity distribution at the point from which the particles are projected in the direction of the wall. Integration is performed only over the particle velocities directed towards the wall. Following Binder and Hanratty (1992), $p(v)$ is assumed to be Gaussian. With this assumption it follows that

$$v \cdot C = \frac{1}{2}\sqrt{\frac{2}{\pi}}\sqrt{\langle v_p'^2 \rangle} \cdot C, \qquad [20]$$

so that the free-flight velocity v is equal to

$$v = \frac{1}{2}\sqrt{\frac{2}{\pi}}\sqrt{\langle v_p'^2 \rangle}. \qquad [21]$$

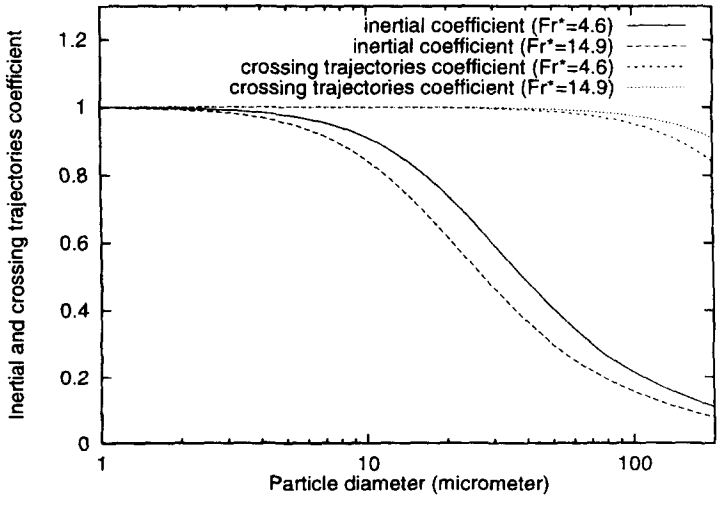

Figure 5. The inertial and crossing trajectories coefficients as a function of particle diameter for Fr* = 4.6 and Fr* = 14.9.

The particle mean square velocity is calculated from the ratio of velocity fluctuations between particle and fluid given in Hinze (1975) (chapter 5.7) in which we have substituted the large density ratio between particle and fluid, leading to

$$\frac{\langle v_p'^2 \rangle}{\langle v_f'^2 \rangle} = \frac{1}{1 + S}. \quad [22]$$

Strictly speaking, the expression given by Hinze is no longer valid for large density ratios due to the possible crossing trajectories effect. However, in our analysis of the crossing trajectories effect it was shown that the effect is rather small for particle sizes under consideration. The relation [22] is also used by Swailes and Reeks (1994). At the beginning of the boundary layers $\sqrt{\langle v_f'^2 \rangle} = 0.9 \cdot u^*$. Then it follows from [21] and [22] that

$$v = \frac{1}{2}\sqrt{\frac{2}{\pi}}\sqrt{\frac{\langle v_f'^2 \rangle}{1 + S}}. \quad [23]$$

Binder and Hanratty (1992) used the following empirical approximation:

$$\frac{\langle v_p'^2 \rangle}{\langle v_f'^2 \rangle} = \frac{1}{1 + \left(\frac{0.7\tau_p}{T_L}\right)}. \quad [24]$$

For Stokes relaxation time, this expression reduces to

$$\frac{\langle v_p'^2 \rangle}{\langle v_f'^2 \rangle} = \frac{1}{1 + 0.7 \cdot S}, \quad [25]$$

having the same form as [22]. They calculated the fluid r.m.s. velocity near the boundaries as $\sqrt{\langle v_f'^2 \rangle} = 0.9 \cdot u^*$, as we did.

We now derive the boundary conditions by applying conservation of mass at the beginning of the boundary layer: the diffusive plus the gravitational flux towards the boundary layer $(D_p(\partial C)/(\partial y) + v_g C)$ must be equal to the free-flight plus the gravitational flux from the boundary layer to the wall $(vC + v_g C)$. Assuming that the boundary layer is thin enough to apply this condition exactly on the wall, we find the diffusion free-flight boundary condition (Binder and Hanratty 1992) at the bottom wall ($y^+ = 0$):

$$D_p^+ \frac{\partial C^+}{\partial y^+} = v^+ C^+. \quad [26]$$

At the top wall ($y^+ = 1$), we have

$$-D_p^+ \frac{\partial C^+}{\partial y^+} = v^+ C^+. \quad [27]$$

A more theoretical discussion and justification of this type of boundary condition is given in Morse and Feshbach (1953) chapter 2.4 (subsection on Boundary Conditions). We remark that the ratio D_p/v is of the order of the particle mean free path. Because the particle mean free path is large compared to the length scale characterizing the variation in the particle concentration, $\partial C/\partial y$, there can be a finite concentration at the wall. For particles with $S \ll 1$ the particle mean free path vanishes at the wall, leading to the boundary condition which normally represents perfect absorption, $C = 0$. To close the one-dimensional model, we consider two initial conditions. The first initial condition is a uniform concentration:

$$C^+(t^+ = 0) = C_0 = 1. \quad [28]$$

The second initial condition is a delta source at the bottom wall:

$$C^+(t^+ = 0) = \delta(y^+). \quad [29]$$

Other initial conditions can be used without problems. The initial source at the bottom is the initial condition that was considered by Binder and Hanratty (1992).

The mathematical formulation of the problem now consists of [13] with boundary conditions [26] and [27] and initial condition [28] or [29].

4. ANALYTICAL SOLUTION OF THE ONE-DIMENSIONAL PROBLEM

Equation (13) with boundary conditions [26] and [27] and initial condition [28] or [29] now can be solved analytically (by separation of variables) leading to a series solution for $C^+(y^+, t^+)$:

$$C^+(y^+, t^+) = \exp\left[-\frac{1}{2}\mathrm{P}y^+\right]\sum_{n=0}^{\infty}\gamma_n[\cos(b_n y^+) + \beta_n \sin(b_n y^+)]\exp(-k_n^2 D_\mathrm{p}^+ t^+). \quad [30]$$

The eigenvalues k_n are determined by the boundary conditions. We have defined the eigenvalues k_n in terms of b_n:

$$k_n^2 := b_n^2 + \left(\frac{1}{2}\mathrm{P}\right)^2, \quad [31]$$

where b_n then satisfies the transcendental equation

$$\tan b_n = \frac{2\lambda b_n}{(a^2 - \lambda^2) + b_n^2}. \quad [32]$$

λ is the dimensionless free-flight/diffusion ratio equal to vH/D_p. γ_n is used to satisfy the initial condition, and is given by

$$\gamma_n = \frac{\int_0^1 C^+(t=0)\mathrm{e}^{ay^+}(\cos b_n y^+ + \beta_n \sin b_n y^+)\,\mathrm{d}y^+}{\int_0^1 \mathrm{e}^{2ay^+}(\cos b_n y^+ + \beta_n \sin b_n y^+)^2\,\mathrm{d}y^+}. \quad [33]$$

γ_n can be solved analytically. For $C^+(t=0) = \delta(y^+)$ the numerator in [33] is equal to 1. Furthermore, we have defined

$$a := -\frac{1}{2}\mathrm{P}, \quad [34]$$

and

$$\beta_n := \frac{\dfrac{vH}{D_\mathrm{p}} + \dfrac{1}{2}\mathrm{P}}{b_n}. \quad [35]$$

Table 4 gives the properties of particles that are used in the Turbulent Diffusion Model. The first values given in each row are at $V_\mathrm{G} = 32$ m/s ($\mathrm{Fr}^* = 4.6$), the second values are given at $V_\mathrm{G} = 62$ m/s ($\mathrm{Fr}^* = 14.9$). Table 5 gives the properties of the fluid that are used in the Turbulent Diffusion Model. $\mathrm{Re}_\mathrm{f}^* = u^*H/\nu_\mathrm{f}$ and $\mathrm{Fr}^* = (u^*)^2/gH$.

The solution $C^+(y^+, t^+)$ given by [30] depends on three physical parameters: the Peclet number P, the dimensionless free-flight/diffusion ratio vH/D_p (determining the boundary conditions), and the initial condition $C^+(t=0) = C_0$. In figures 6 and 7 we have plotted the one-dimensional concentration profiles for 50 and 100 μm particles and $\mathrm{Fr}^* = 14.9$ at different distances travelled downstream. The initial condition is the uniform concentration. If it is assumed that droplets travel axially at a constant velocity, this distance travelled downstream is easily found by multiplying the time by the gas velocity. Convergence of the series in [30] is achieved by taking 100 terms into account and calculating the concentration in a simple FORTRAN program. The smaller the value of the time t, the more terms are needed in the series.

For the 50 μm particles the turbulent diffusion is relatively large, leading to a positive concentration gradient at the bottom wall. As a result of this deposition, due to turbulence the maximum in the concentration profile is above the bottom wall. Figure 6 shows that it takes more than 600 channel diameters travelled downstream before all the particles are deposited. A small

Table 4. Properties of the particles that are used in the Turbulent Diffusion Model. First values are for 32 m/s gas velocity (Fr* = 4.6), second values are for 62 m/s gas velocity (Fr* = 14.9)

d_p (μm)	τ_p (s)	τ_p^+	D_p (m^2/s)	γ^{inert}	γ_{cross}	v_g (m/s)	v (m/s)	P	S	H/l
10	3.3×10^{-4}	44	1.6×10^{-3}	0.91	1	3.2×10^{-3}	0.49	0.4	0.2	8.7
		142	2.4×10^{-3}	0.84	1		0.82	0.1	0.4	8.4
50	8.25×10^{-3}	1092	7.0×10^{-4}	0.40	1	8.1×10^{-2}	0.21	5.8	5.2	5.1
		3538	8.7×10^{-4}	0.30	1		0.29	4.7	10.2	4.1
100	0.033	4370	3.6×10^{-4}	0.22	0.99	0.32	0.11	42	21	2.9
		14.150	4.3×10^{-4}	0.15	1		0.15	38	41	2.2
200	0.13	17.200	1.8×10^{-4}	0.11	0.93	1.27	0.06	354	82	1.7
		55.700	2.3×10^{-4}	0.08	0.98		0.08	277	160	1.3

Table 5. Properties of the fluid that are used in the Turbulent Diffusion Model

V_G (m/s)	Re_f	Re_f^*	Fr*	T_L (s)	u^* (m/s)	D_f (m^2/s)
32	94.118	4412	4.6	1.6×10^{-3}	1.5	1.76×10^{-3}
62	182.353	7941	14.9	8.1×10^{-4}	2.7	2.9×10^{-3}

amount of the particles deposit at the top wall. For 100 μm particles the relative importance of turbulent diffusion is much less. The maximum in the concentration profile therefore lies much closer to the bottom wall than for 50 μm particles, as is seen in figure 7. This figure also shows that, although the initial distribution is uniform, the concentration profiles for the 100 μm particles show that the particles very rapidly fall to the bottom part of the channel and there is no deposition at the top of the channel. Within 20 channel diameters downstream all the particles are deposited at the bottom wall.

Figures 8 and 9 give the concentration profiles for the delta source at the bottom as the initial particle distribution. Comparison of figures 6 and 7 with figures 8 and 9 shows that for the delta source at the bottom it takes less time before all the particles are deposited than for the uniform initial distribution. Furthermore, almost no particles deposit at the top wall whereas in the case of the uniform initial distribution there are particles depositing at the top wall. The concentration profiles become independent of the initial condition after a certain time. This is, of course, what we expect.

The deposition flux R_D is given by the sum (for the bottom wall) or the difference (for the top wall) of the free-flight flux and the gravitational settling flux:

$$R_D = (v \pm v_g)C. \qquad [36]$$

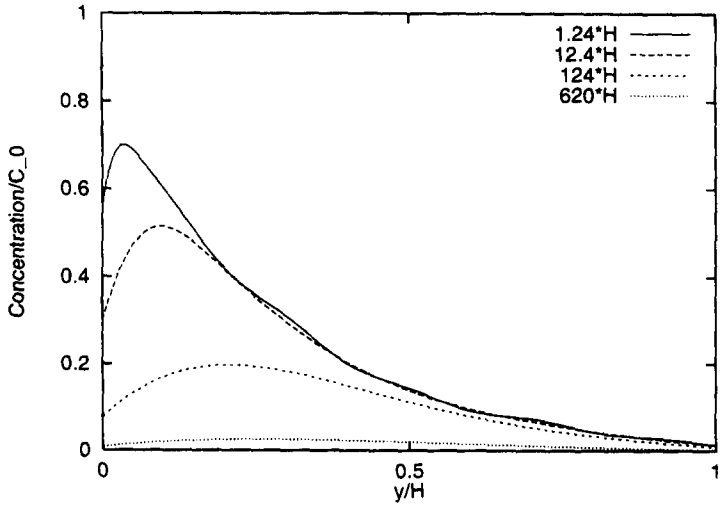

Figure 6. Concentration profiles at different distances travelled downstream (expressed in the number of channel heights) for 50 μm particles (S = 10.2) and for Fr* = 14.9; uniform initial distribution.

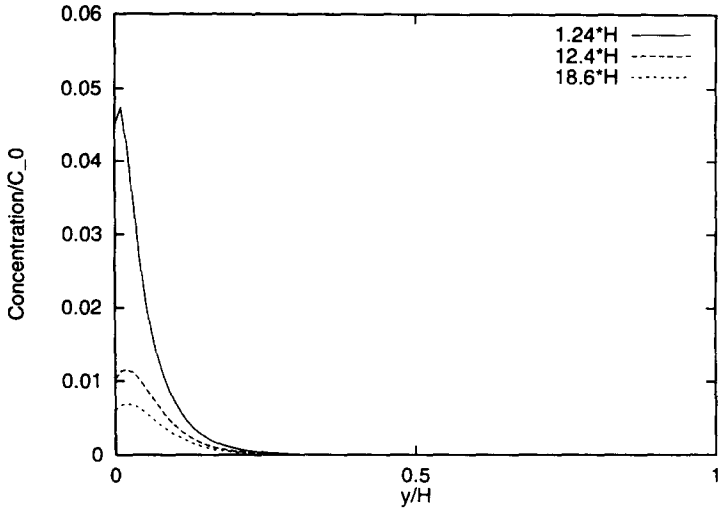

Figure 7. Concentration profiles at different distances travelled downstream (expressed in the number of channel heights) for 100 μm particles (S = 41) and for Fr* = 14.9; uniform initial distribution.

For $v_g > v$, the deposition flux at the top is equal to 0. The ratio $D_{rel}(t^+)$ of deposition fluxes at the top and at the bottom then follows straight from the solution for the concentration and [36]:

$$D_{rel}(t^+) = \frac{v - v_g}{v + v_g} \exp\left[-\frac{1}{2}\mathrm{P}\right] \frac{\sum_{n=0}^{\infty} \gamma_n(\cos(b_n) + \beta_n \sin(b_n))\exp(-k_n^2 D_p^+ t^+)}{\sum_{n=0}^{\infty} \gamma_n \exp(-k_n^2 D_p^+ t^+)}. \quad [37]$$

Only for free-flight velocities larger than the gravitational settling velocity can particles deposit at the top wall. In the limit $t \to \infty$, when the initial condition does not affect the solution anymore, D_{rel} is equal to

$$D_{rel} = \frac{v - v_g}{v + v_g} \exp\left[-\frac{1}{2}\mathrm{P}\right]. \quad [38]$$

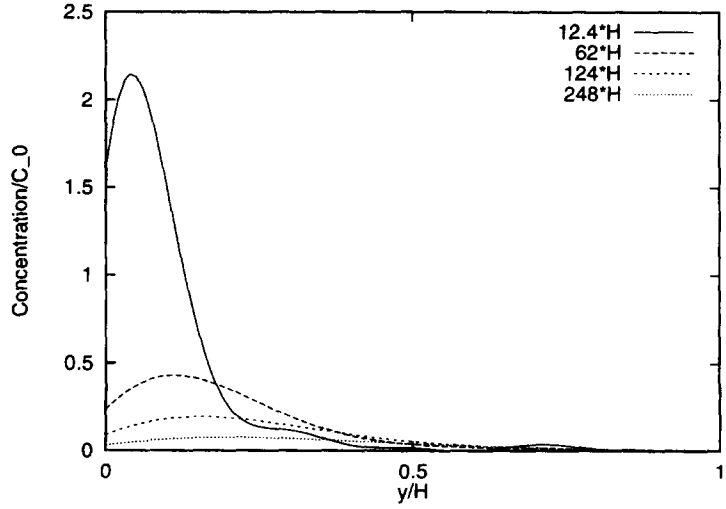

Figure 8. Concentration profiles at different distances travelled downstream (expressed in the number of channel heights) for 50 μm particles (S = 10.2) and for Fr* = 14.9; initial delta source at the bottom.

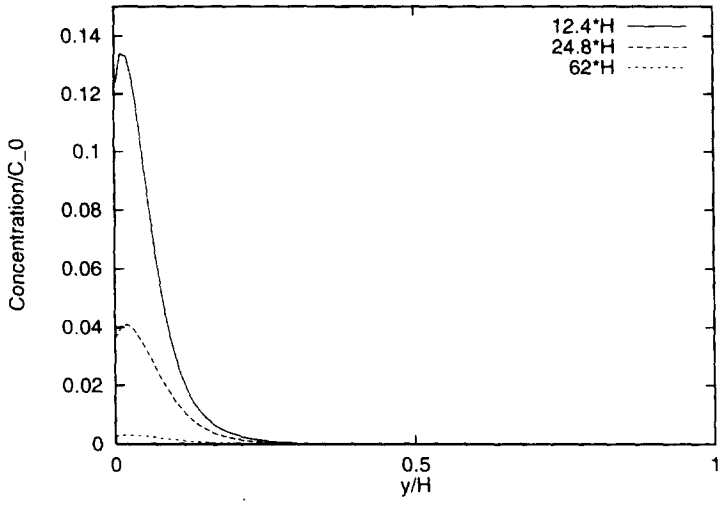

Figure 9. Concentration profiles at different distances travelled downstream (expressed in the number of channel heights) for 50 μm particles (S = 41) and for Fr* = 14.9; initial delta source at the bottom.

In figure 10 we have plotted this D_{rel} as a function of the height between the horizontal plates and the particle diameter. Particles larger than 70 μm are, in the absence of any initial velocity, not able to reach the top wall. 10 μm particles (the minimum size of particles in this model) deposit in almost equal amounts at the top and at the bottom. Between 10 and 70 μm the relative deposition quickly drops to zero.

How does the relative deposition change with increasing Froude number? In figure 11 we have plotted the relative deposition of particles in the cases of Fr* = 4.6 and Fr* = 14.9 and a channel height of 5×10^{-2} m. Note that the curve for Fr* = 14.9 lies only slightly above the one for Fr* = 4.6. This is due to two effects which compensate each other to a certain extent. For a higher gas velocity, and therefore a higher Froude number, the correlation time T_L decreases, leading to a larger Stokes number, and a decreasing particle diffusivity as a result of the inertia effect. On the other hand, the particle diffusivity increases due to the increasing fluid diffusivity. The latter increases more than the former decreases, so that, according to [15], the net particle diffusivity increases slightly going to higher Froude numbers. We see that for the whole range of Fr* numbers between 4.6 and 14.9 the relative deposition rapidly drops to zero between 10 and 70 μm.

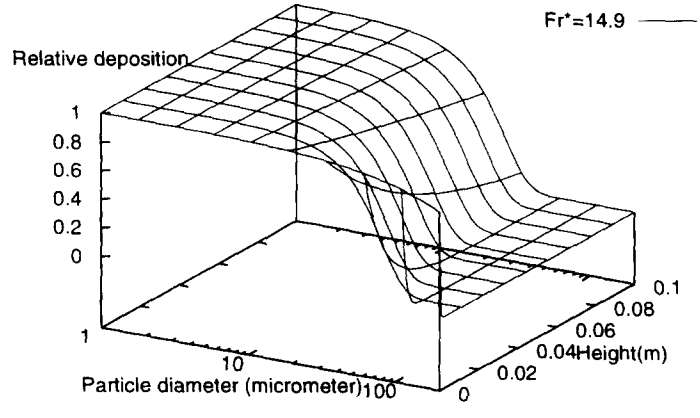

Figure 10. Relative deposition of particles between the top and the bottom of the channel as a function of particle diameter and height of the channel.

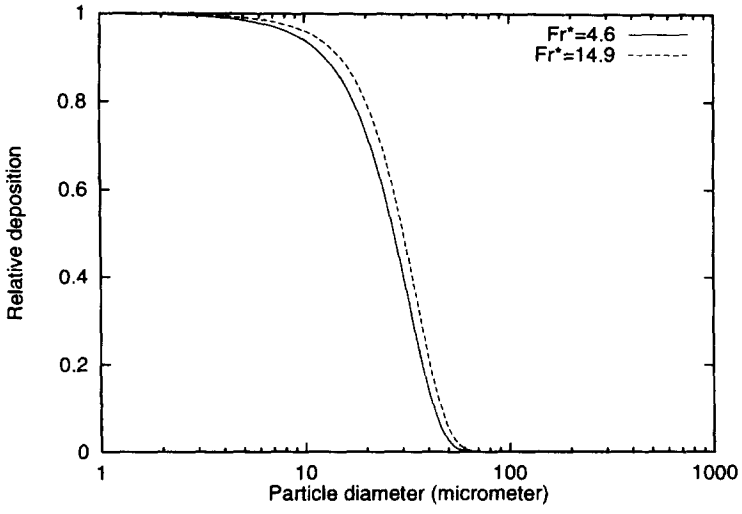

Figure 11. Comparison between the relative deposition of particles between the top and the bottom of the channel as a function of the particle diameter for Fr* = 4.6 and Fr* = 14.9.

5. EXTENSION TO A TWO-DIMENSIONAL DEPOSITION FLUX AND COMPARISON WITH A SEMI-EMPIRICAL CORRELATION

Paras and Karabelas (1991) found in their experiment with a horizontal annular dispersed gas/liquid flow in a 5 cm tube that the concentration of particles on a horizontal line in the cross-section of the tube is more or less constant. Using this experimental result as an extra assumption, our one-dimensional model then can be extended to a quasi two-dimensional model by substituting

$$y^+ = \frac{y}{d_t} \rightarrow \frac{1}{d_t}\cdot\left(\frac{1}{2}d_t(1-\cos\phi)\right) = \frac{1}{2}(1-\cos\phi)$$

in $R_D^+(\phi, t^+) = (v^+ + v_g^+)C^+(y^+, t^+)$, where $C^+(y^+, t^+)$ is given in [30]. d_t is the diameter of the tube. Furthermore, we substitute $v_g^+ \rightarrow v_g^+ \cos\phi$ in the expression for the deposition flux. This leads to

$$R_D^+(\phi, t^+) = [v^+ + v_g^+\cos\phi]\exp\left[\frac{1}{4}\mathrm{P}(\cos\phi - 1]\right]$$

$$\cdot\sum_{n=0}^{\infty}\gamma_n\left[\cos\left(\frac{1}{2}b_n(1-\cos\phi)\right) + \beta_n\sin\left(\frac{1}{2}b_n(1-\cos\phi)\right)\right]\exp(-k_n^2 D_p^+ t^+). \quad [39]$$

As we have assumed turbulence to be homogeneous, the free-flight velocity is independent of ϕ. The series in expression [39] is not of a genuine physical origin for our two-dimensional case. As can be seen in figure 6, the maximum in the concentration profile in the one-dimensional case is above the bottom wall. Therefore, the result [39] leads to a local minimum at $\phi = 0$ and local maxima at ϕ values slightly larger than 0. This is an artificial effect. As the series term in [39] is a term depending on the initial entrainment condition (via γ_n), we propose to write it for the stationary case as some unknown constant c_E, to be determined by the initial entrainment condition. c_E will generally differ for different particle relaxation times. The final result for the two-dimensional deposition flux that follows from our analysis can then be written as

$$R_D(\phi, \tau_p) = k_D(\phi, \tau_p)\cdot\exp\left(\frac{1}{4}\mathrm{P}(\cos\phi - 1)\right), \quad [40]$$

where the local deposition constant $k_D(\phi, \tau_p)$ is defined as

$$k_D(\phi, \tau_p) = c_E(\tau_p) \cdot (v + v_g \cos \phi), \quad [41]$$

having the dimension of velocity. The constant c_E can be determined from the fact that in a fully developed annular gas/liquid flow the total entrainment flux equals the total deposition flux:

$$\int_0^\pi R_E(\phi, \tau_p)\, d\phi = \int_0^\pi R_D(\phi, \tau_p)\, d\phi. \quad [42]$$

From [40], [41] and [42] it follows that

$$c_E(\tau_p) = \frac{\int_0^\pi R_E(\phi, \tau_p)\, d\phi}{\int_0^\pi (v + v_g \cos \phi) \exp\left(\frac{1}{4} P(\cos \phi - 1)\right) d\phi}. \quad [43]$$

In figure 12 we have plotted the deposition flux of [40] normalized by c_E for two Froude numbers as a function of the circumferential tube angle for four different particle sizes: 10, 50, 100 and 200 μm particles. Although we have plotted these curves in one figure, we recall that c_E is generally different for different particle relaxation times. This means that for each particle relaxation time the curves in figure 12 have to be multiplied by a different multiplication factor c_E with respect to the horizontal axis.

Figure 12 shows that 50 μm particles are just able to deposit up to the top of the tube, 100 μm particles can only deposit up to one third of the tube wall circumference, and 200 μm particles deposit up to one sixth of the tube wall circumference. The smaller the particle size, the broader the curve for the deposition flux. This is easily explained by the fact that as the influence of gravity becomes less, particles deposit more and more uniformly around the tube circumference. The width (defined by the angle at which the deposition flux is at $1/e$ of its value at the bottom) of the deposition curves is mainly determined by $\frac{1}{4}$P. The width decreases if the Peclet number increases. The Peclet number increases if the acceleration of gravity and/or the radius of the tube increases, and/or if the particle diffusion coefficient decreases. In the limit P $\rightarrow$ 0 the influence of gravity is negligible and R_D (ϕ) becomes a constant independent of ϕ. In the limit P $\rightarrow \infty$ the influence of gravity is infinite, and there can only be deposition at the bottom of the tube, at least in the framework of our model, where particles do not have an initial entrainment velocity.

The influence of the Froude number on the deposition flux is also shown in this figure. The smaller the size of the particle, the larger the influence of a change in the Froude number. Again,

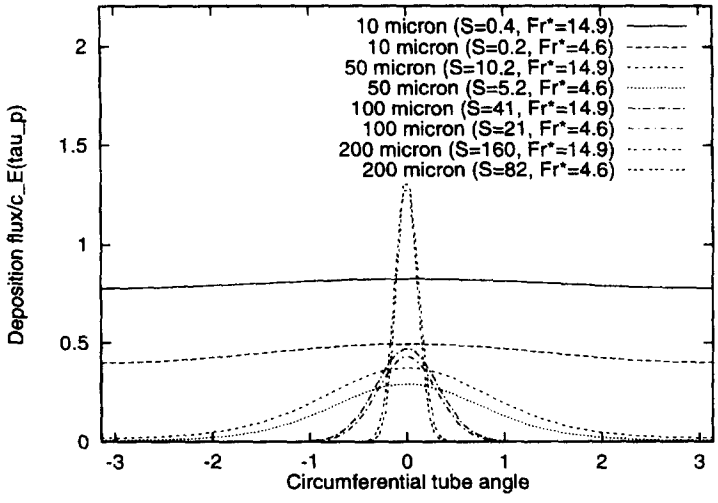

Figure 12. Deposition flux normalized by $c_E(\tau_p)$ vs circumferential tube angle for four different particle sizes and for Fr* = 4.6 and Fr* = 14.9; the Stokes number S is given as well for the particles.

this is an effect which can be expected on the basis of the fact that for smaller particles the influence of turbulent diffusion is relatively large in comparison with the influence of gravity. For a larger Froude number the deposition flux at a certain ϕ is larger. For the 10 μm particles it is almost twice as much in figure 12, but this effect decreases with increasing particle relaxation time. For the 100 and 200 μm particles this effect is very little. This is due to the fact that for larger gas velocities the effect of an increasing fluid diffusion coefficient is partly compensated by a decreasing inertial coefficient (see table 4). Analysis of [40] thus shows that its behaviour is, at least qualitatively, in accordance with what is physically expected.

We recall the semi-empirical correlation given in Laurinat *et al.* (1985):

$$R_D(\phi) = k_D[1 + 10 \exp(2(\cos\phi - 1))]. \quad [44]$$

In this expression k_D is a constant (with the dimensions of velocity) that has to be calculated from the entrainment flux of particles $R_E(\phi)$ according to

$$k_D = \frac{\int_0^\pi R_E \, d\phi}{\int_0^\pi C_W \, d\phi}. \quad [45]$$

C_W is the concentration at the wall at a position ϕ. Correlation [44] is the result of deposition of particles with different particle sizes. We can write a general correlation of the form [44] as

$$R_D(\phi) = k_D[1 + A \exp(B(\cos\phi - 1))], \quad [46]$$

and a general correlation of the form [40] as

$$R_D(\phi) = k_D(\phi)\exp(B(\cos\phi - 1)) = c_E A(\phi)\exp(B(\cos\phi - 1)). \quad [47]$$

Let us now compare our result [47] with the semi-empirical correlation [46]. We note three differences. The first difference in form between [46] and [47] is an offset constant which takes the value k_D in [46]. The physical interpretation of this offset constant can be the deposition of particles with $S \ll 1$. These particles are not influenced by gravity and therefore deposit uniformly around the circumference of the tube. A second difference is that k_D is independent of ϕ in [46], whereas our analysis indicates that it should depend on ϕ. Our result is in accordance with recent work by Williams *et al.* (1996), who have assumed that the local deposition constant k_D is ϕ-dependent:

$$k_D(\phi) = \frac{C_W(\phi)}{C_B}[v + v_g \cos\phi]. \quad [48]$$

Here, C_B is the bulk concentration and C_W is the wall concentration, which generally depends on ϕ. From our analysis it follows that C_W is proportional to $\exp(\frac{1}{4}P(\cos\phi - 1))$.

$A(\phi)$ in [47] is defined as

$$A(\phi) = v + v_g \cos\phi. \quad [49]$$

A third difference is the explicit form of B in [47] that follows from our analysis. B is found to be determined by the ratio between convection and diffusion terms according to

$$B := \frac{1}{4}P. \quad [50]$$

Instead of the empirical constants for A and B in [44], we have found with [49] and [50] how they depend on the relevant physical parameters in the problem. It should be noted again that Laurinat's correlation is the result of integrating over all particle relaxation times present in a horizontal annular dispersed gas/liquid flow. If the distribution over particle relaxation times is given as $n(\tau_p)$, we can use it in order to calculate from our result [40] the average deposition flux according to

$$\langle R_D(\phi)\rangle = \int R_D(\phi, \tau_p) n(\tau_p) \, d\tau_p. \quad [51]$$

The expression [40] derived for the two-dimensional deposition flux is an expression for the deposition flux on the one hand depending on experimental information of the entrainment process (via c_E), but on the other hand explicitly containing the relevant physical parameters of the deposition problem (via $(v + v_g \cos\phi)$ and P).

The physical variables which totally determine the solution of the Turbulent Diffusion Model [40] are: acceleration of gravity, particle relaxation time, integral fluid time scale, tube diameter, mean square fluid velocity and the Eulerian length scale. Particle time scale, integral fluid time scale and fluid mean square velocity are in fact microscopic, dependent parameters. As we have neglected the influence of the liquid film in our problem, the total solution depends, for a given particle/fluid density ratio, on the following macroscopic parameters: acceleration of gravity, tube diameter and average gas velocity. The Froude number is the characteristic dimensionless number that can be constructed from these three parameters. The distribution of particle relaxation times is determined by the Froude number and the superficial liquid velocity, in a way which is yet unknown. It is only known qualitatively that with increasing gas velocity the particle mean diameter decreases rapidly, whereas with increasing superficial liquid velocity the particle diameter decreases at low gas velocities, but increases at high gas velocities (Hay *et al.* 1996). The influence of the Froude number on the particle size distribution is dominant over the influence of the superficial liquid velocity.

Now, we would like to transform [40] into an equation which only contains the macroscopic, independent variables: acceleration of gravity, average gas velocity and tube diameter. The Eulerian length scale can be estimated from the tube diameter, and the fluid mean square velocity from the friction velocity. From the resulting parameters τ_p, T_L, u^*, g, d_t, two dimensionless groups can be formed: $S = \tau_p/T_L$ and $Fr^* = (u^*)^2/gd_t$. They also determine the Peclet number P and the dimensionless ratio between free-flight velocity and diffusivity (vd_t/D_p) that occur in the solution [30]. These groups were already recognized by Binder and Hanratty (1992). It follows from [14]–[17] that, neglecting the crossing trajectories effect, the Peclet number is written as

$$P = \frac{2.0 \cdot S\sqrt{1+S}}{Fr^*} \qquad [52]$$

if we assume that $\langle v_f'^2 \rangle = (0.7 \cdot u^*)^2$.

The Eulerian length scale is determined by the tube diameter according to

$$L \approx \frac{1}{10} d_t. \qquad [53]$$

The fluid integral time scale can be estimated from the gas velocity:

$$T_L \approx \frac{d_t}{V_G}. \qquad [54]$$

The fluid Reynolds number determines the friction coefficient, and from this the friction velocity can be calculated. The friction velocity enables us to calculate the fluid mean square velocity:

$$\langle v_f'^2 \rangle = (0.7 \cdot u^*)^2 = 0.02\left(\frac{d_t}{\nu_f}\right)^{-1/4} V_G^{7/4}, \qquad [55]$$

where ν_f is the kinematic viscosity of the fluid and V_G the average gas velocity. Substituting [54] and [55] into [16], the diffusion coefficient of the fluid can be written as

$$D_f = 0.02 \cdot \nu_f^{1/4} d_t^{3/4} V_G^{3/4}. \qquad [56]$$

Substituting [53]–[55] and [22] into [49] and [50] gives A and B in terms of macroscopic variables. Only the particle relaxation time is still present in these expressions.

$$A(V_G, \tau_p, \phi) = g\tau_p \cos\phi + 0.07 \frac{\left(\frac{\nu_f}{d_t}\right)^8 V_G^{7/8}}{\sqrt{1 + \frac{\tau_p \cdot V_G}{d_t}}}, \qquad [57]$$

$$B(V_G, \tau_p) = \frac{12.5 \cdot g\tau_p d_t^{1/4}}{\nu_f^{1/4} V_G^{3/4}} \sqrt{1 + \frac{\tau_p V_G}{d_t}} \sqrt{1 + \left(\frac{10 g\tau_p}{V_G}\right)^2}. \qquad [58]$$

6. CONCLUDING REMARKS

6.1. *Summary*

A Turbulent Diffusion Model has been used to predict the particle deposition flux in a horizontal turbulent tube flow. The new aspects of this Turbulent Diffusion Model are that we have found a one-dimensional analytical solution which can be used to calculate an approximate two-dimensional solution for the deposition flux. We have used a particle diffusion coefficient with an inertial and a crossing trajectories effect and we have calculated these effects quantitatively.

For the one-dimensional case, we have used the analytical solution for the particle concentration to calculate the relative deposition between the top and the bottom wall. We have investigated how this relative deposition depends on the tube diameter, the particle size and the Froude number. For a certain tube diameter, the curve of the relative deposition for $Fr^* = 14.9$ lies only slightly above the one for $Fr^* = 4.6$. This is due to two partly compensating effects: a decreasing inertial coefficient and an increasing fluid diffusivity. The latter increases more than the former decreases, so that the total particle diffusivity increases slightly with increasing gas velocity. We also conclude that for the whole range of Fr^* numbers between 4.6 and 14.9 the relative deposition flux rapidly drops from one to zero between particle diameters 10 and 70 μm.

Subsequently, the analytical solution for the particle concentration to the one-dimensional problem is used to calculate the deposition flux in a tube flow. The physical parameters are found which determine the form of the deposition flux. These were not apparent in the semi-empirical correlation of Laurinat [1]. The general form of the deposition flux that we have derived can be expressed as

$$R_D(V_G, \tau_p, \phi) = c_E(\tau_p) \cdot A(V_G, \tau_p, \phi) \cdot \exp(B(V_G, \tau_p)(\cos \phi - 1)). \quad [59]$$

Here, c_E is determined by the entrainment flux, A is equal to the sum of gravitational settling velocity and free-flight velocity to the wall, and $B = \frac{1}{4}P$, with P the dimensionless number characterizing the convection/diffusion ratio. P can be expressed in terms of the Froude number and the Stokes number. If the specific particle size distribution is known, the average deposition flux can be found by integrating [59] over the particle relaxation time. Correlations which have been developed up till now did not contain the relevant physical parameters of the problem. The ϕ dependency in A and the dependency on the gas velocity in A and B, which result from our analysis, have not been quantified in previous work. The influence of the Froude number on the deposition flux for four different particle sizes has been investigated. The maximum circumferential angle in the tube up to which particles of a certain size can deposit is predicted for an air–water annular flow in a tube with a diameter of 5×10^{-2} m. Particles larger than about 70 μm are not able to reach the top of the tube without having an initial radial entrainment velocity. The influence of the crossing trajectories effect on the particle diffusion coefficient has been calculated, and it is found that only for particles larger than about 150 μm can the effect become significant in a horizontal annular dispersed gas/liquid flow.

6.2. *Discussion*

We will now reconsider the assumptions on which our Turbulent Diffusion Model is based. The average fluid velocity will not be uniform over the whole cross-section of the tube, as has been assumed, but only over about 80% of the tube diameter. Turbulence will also be inhomogeneous close to the walls. This would on the one hand lead to a turbophoresis effect, resulting in an extra deposition flux, but on the other hand, especially the smaller particles ($\tau^+ < 10$) can become trapped in the boundary layer. The turbulent fluctuations here become too small to support the motion of the small particles to the wall. However, it is expected that the high inertia particles that we consider effectively see homogeneous turbulence. The local equilibrium assumption is questionable, because of the inhomogeneous turbulence. Actually, another transport equation than a Fickean diffusion equation is needed which is not restricted to homogeneous turbulence and large particle relaxation times. This is the PDF kinetic equation (Reeks 1991, 1992). Furthermore, the particle free fall velocity and the particle diffusion coefficient will initially be time-dependent, and only when particles have been for some time in the flow field will they become constant.

The diffusion free-flight boundary condition is a phenomenological model. It is not clear where the starting point of the free-flight process has to be taken and what the value of the free-flight velocity at this point is. The velocity distribution at the beginning of the boundary layer is taken to be Gaussian. In figure 6 in Swailes and Reeks (1994) it can be seen that the velocity distribution close to the wall deviates from a real Gaussian. The p.d.f. function is shifted towards velocities directed from the wall. Figure 11 in the same article shows how the particle r.m.s. velocity decreases in the direction of the wall, purely as a result of the wall effect. The particle r.m.s. velocity can be about 20% lower than that in the centre of the tube. The actual boundary condition is a constraint on the velocity, whereas in the Turbulent Diffusion Model there is no information on the velocity. A PDF kinetic model is needed to model the boundary conditions in a more natural way. In horizontal annular dispersed gas/liquid flow in a tube there is a liquid film at the wall, which changes the boundary conditions, and will lead to an enhanced deposition of the small particles. Deposition of large particles is not influenced by the presence of a liquid film. The presence of a (wavy) liquid film will also increase the interfacial friction by 5%–10% (Laurinat 1982). This will increase the turbulence intensities, and therefore the diffusivities of the particles. The volume fraction of the droplets is $O(10^{-3})$, so that the droplets surely influence the turbulence (two way coupling), and turbulence could be reduced. The range of droplet diameters is generally between 10 and 1000 μm. For particles with a stopping distance of the order of, or larger than, the tube diameter (particles larger than 200 μm), the initial entrainment momentum is very important. Theoretically, however, little is known about this initial entrainment momentum. The volume fraction of droplets smaller than 10 μm is very small compared to the volume fraction of droplets larger than 10 μm. Because they have small Peclet numbers, they will deposit uniformly around the circumference of the tube.

Despite these idealizations, an expression of the form [59] is believed to enlarge the understanding of the deposition process in a horizontal annular dispersed gas/liquid flow and to be useful in developing new semi-empirical correlations for the deposition flux. Analysis of the deposition flux that we have derived showed that at least qualitatively it behaves in a way that is physically expected.

Acknowledgements—This work has been supported by Stichting voor Fundamenteel Onderzoek der Materie (Foundation for Fundamental Research on Matter, FOM).

REFERENCES

Anderson, R. J. and Russell, T. W. F. (1970) Circumferential variation of interchange in horizontal annular two-phase flow. *Ind. Eng. Chem. Fundam.* **9,** 340–344.

Binder, J. L. and Hanratty, T. J. (1992) Use of Lagrangian methods to describe drop deposition and distribution in horizontal gas–liquid annular flows. *Int. J. Multiphase Flow* **18,** 803–820.

Chesters, A. K. (1975) The applicability of dynamic similarity criteria to isothermal, liquid–gas, two-phase flows without mass transfer. *Int. J. Multiphase Flow* **2,** 191–212.

Csanady, G. T. (1963) Turbulent diffusion of heavy particles in the atmosphere. *J. Atmospheric Sci.* **20,** 201–208.

Friedlander, S. K. and Johnstone, H. F. (1957) Deposition of suspended particles from turbulent gas streams. *Ind. Eng. Chem.* **47,** 1151–1156.

Fukano, T. and Ousaka, A. (1989) Prediction of the circumferential distribution of film thickness in horizontal and near-horizontal gas–liquid annular flows. *Int. J. Multiphase Flow* **15,** 403–419.

Hay, K. J., Liu, Z.-C. and Hanratty, T. J. (1996) Relelation of deposition to drop size when the rate law is nonlinear. *Int. J. Multiphase Flow* **22,** 829–848.

Hinze, J. O. (1975) *Turbulence*. McGraw-Hill, New York.

James, P. W., Wilkes, N. S., Conkie, W. and Burns, A. (1987) Developments in the modelling of horizontal annular two-phase flow. *Int. J. Multiphase Flow* **13,** 173–198.

Kallio, G. A. and Reeks, M. W. (1989) A numerical simulation of particle deposition in turbulent boundary layers. *Int. J. Multiphase Flow* **15,** 433–446.

Laurinat, J. E. (1982) Studies of the effects of pipe size on horizontal annular two-phase flows. Ph.D. Thesis, University of Illinois at Urbana-Champaign, Urbana, IL.

Laurinat, J. E., Hanratty, T. J. and Jepson, W. P. (1985) Film thickness distribution for gas–liquid annular flow in a horizontal pipe. *Phys. Chem. Hydrodynam.* **6,** 179–195.

Morse, P. M. and Feshbach, H. (1953) *Methods of Theoretical Physics*. McGraw-Hill, New York.

Paras, S. V. and Karabelas, A. J. (1991) Droplet entrainment and deposition in horizontal annular flow. *Int. J. Multiphase Flow* **17,** 455–468.

Reeks, M. W. (1983) The transport of discrete particles in inhomogeneous turbulence. *J. Aerosol Sci.* **14,** 729–739.

Reeks, M. W. (1991) On a kinetic equation for the transport of particles in turbulent flows. *Phys. Fluids* **3,** 446–456.

Reeks, M. W. (1992) On the continuum equations for dispersed particles in nonuniform flows. *Phys. Fluids* **4,** 1290–1303.

Swailes, D. C. and Reeks, M. W. (1994) Particle deposition from a turbulent flow. I. A steady-state model for high inertia particles. *Phys. Fluids* **6,** 3392–3403.

Taylor, G. I. (1921) Diffusion by continuous movements. *Proceedings of the London Mathematical Society*, Vol. 2, pp. 196–212.

Uijttewaal, W. S. J. and Oliemans, R. V. A. (1996) Particle dispersion and deposition in direct numerical and large eddy simulations of vertical pipe flows. *Phys. Fluids* **8,** 2590–2604.

Vames, J. S. and Hanratty, T. J. (1988) Turbulent dispersion of droplets for air flow in a pipe. *Exp. Fluids* **6,** 94–104.

Williams, L. R., Dykhno, L. A. and Hanratty, T. J. (1996) Droplet flux distributions and entrainment in horizontal gas–liquid flows. *Int. J. Multiphase Flow* **22,** 1–18.